Eurasian Journal of Physics and Functional Materials

Volume 9 | Number 1

Article 6

Pages: 48 - 54

3-29-2025

Synthesis and characterization of electrolyte and electrode material sample for solid oxide fuel cells

Kenzhebatyr Bekmyrza
Institute of Physical and Technical Sciences, L.N. Gumilyov Eurasian National University, Astana 010008, Kazakhstan

Aliya Baratova
Institute of Physical and Technical Sciences, L.N. Gumilyov Eurasian National University, Astana 010008, Kazakhstan, baratova_aa@enu.kz

Gulshat A. Bakalbayeva
Institute of Physical and Technical Sciences, L.N. Gumilyov Eurasian National University, Astana 010008, Kazakhstan

Marzhan M. Kubenova
Faculty of Transport and Energy, L.N. Gumilyov Eurasian National University, Astana 010008, Kazakhstan

Gaukhar Kabdrakhimova
Institute of Physical and Technical Sciences, L.N. Gumilyov Eurasian National University, Astana 010008, Kazakhstan

See next page for additional authors

Recommended Citation

Bekmyrza, Kenzhebatyr; Baratova, Aliya; Bakalbayeva, Gulshat A.; Kubenova, Marzhan M.; Kabdrakhimova, Gaukhar; Kabyshev, Asset Zh.; and Kuterbekov, Kairat (2025) "Synthesis and characterization of electrolyte and electrode material sample for solid oxide fuel cells," *Eurasian Journal of Physics and Functional Materials*: Vol. 9: No. 1, Article 6.
DOI: https://doi.org/10.69912/2616-8537.1242

Synthesis and characterization of electrolyte and electrode material sample for solid oxide fuel cells

Authors

Kenzhebatyr Bekmyrza, Aliya Baratova, Gulshat A. Bakalbayeva, Marzhan M. Kubenova, Gaukhar Kabdrakhimova, Asset Zh. Kabyshev, and Kairat Kuterbekov

ORIGINAL STUDY

Synthesis and Characterization of Electrolyte and Electrode Material Sample for Solid Oxide Fuel Cells

Kenzhebatyr Bekmyrza [a], Aliya Baratova [a,*], Gulshat A. Bakalbayeva [a], Marzhan M. Kubenova [b], Gaukhar Kabdrakhimova [a], Asset M. Kabyshev [a], Kairat Kuterbekov [a]

[a] Institute of Physical and Technical Sciences, L.N. Gumilyov Eurasian National University, Astana 010008, Kazakhstan
[b] Faculty of Transport and Energy, L.N. Gumilyov Eurasian National University, Astana 010008, Kazakhstan

Abstract

The synthesis of electrolytes based on nanopowders of $Zr_{0.84}Y_{0.16}O_2$-δ (YSZ), $Zr_{0.81}Sc_{0.19}O_2$-δ (ScSZ), and $Ce_{0.73}Gd_{0.27}O_2$-δ (GDC) was carried out using laser evaporation. The resulting powders had average particle sizes of 15.5 μm (YSZ), 11.0 μm (ScSZ), and 0.02 μm (GDC), as determined by BET analysis. The specific surface areas of the powders were 65.3 m^2/g for YSZ, 97.4 m^2/g for ScSZ, and 34.2 m^2/g for GDC. Additionally, cathode material powders of $La_{0.7}Sr_{0.3}MnO_3$ (LSM) and lanthanum strontium cobalt ferrites (LSCF-2020, LSCF-4020, and LSCF-4080) were synthesized using polymer-salt pyrolysis and solution combustion synthesis methods. The LSM powder exhibited a rhombohedral phase (space group R-3c) with a secondary phase content of ~9 wt.%. The LSCF powders demonstrated a single-phase perovskite structure with a rhombohedral symmetry (space group R-3c). Nickel oxide (NiO) powder for the anode was obtained using the wire explosion method, producing predominantly spherical particles. The phase composition of the synthesized materials was determined using X-ray diffraction (XRD), confirming a single-phase structure for all powders except LSM, which contained ~9 wt.% of a secondary phase. The sintering behavior was studied to determine optimal processing conditions, revealing that the electrolytes reached high densification levels at 1300 °C, while the electrodes required sintering at 1100−1150°C. The co-sintering approach was developed for fabricating solid oxide fuel cells (SOFCs), allowing for controlled morphology of polymer-ceramic films. Electrochemical performance tests demonstrated the long-term stability and functional viability of the fabricated solid oxide fuel cells components.

Keywords: Solid oxide fuel cells, Electrolyte, Electrode material, Nanopowder

1. Introduction

Currently, the most common method for fabricating solid oxide fuel cells (SOFCs) involves forming a supporting structure followed by the sequential application and sintering of other components [1]. Repeated high-temperature processing complicates and increases the cost of cell fabrication, whereas sintering all SOFC components in a single thermal cycle (co-sintering) offers significant advantages in terms of energy and time savings. However, achieving co-sintering of a heterogeneous multilayered structure with a predetermined morphology is not a trivial task. This challenge was central to the work presented here. The use of nanoscale electrolyte powders, which enable significant control over sintering kinetics without altering other physical properties (such as the coefficient of thermal expansion, conductivity, etc.), contributed to addressing these challenges.

Another important task for successfully achieving the set goal is obtaining highly active electrodes (both cathode and anode). Since the electrochemical processes occurring at SOFC electrodes depend on many factors—such as chemical composition, the morphology of interphase boundaries, and the physicochemical properties of both the electrode and electrolyte—appropriate electrode materials were selected and methods for obtaining the required microstructure were developed. Moreover, the methodology for forming the electrodes is inextricably linked to the overall

Received 28 February 2025; revised 28 February 2025; accepted 8 March 2025.
Available online 29 March 2025

* Corresponding author.
E-mail address: baratova_aa@enu.kz (A. Baratova).

https://doi.org/10.69912/2616-8537.1242

fabrication of the SOFC. Consequently, both the electrolyte and electrode materials were produced and characterized.

The primary method for forming the supporting component of an SOFC is extrusion [2], which involves forcing a viscous mass through a die that defines the geometry and dimensions of the product. Another popular method is the phase inversion method [3,4]. This technique involves bringing a polymer solution into a supersaturated state, causing the polymer to transition from a liquid to a solid state. After fabricating the supporting component, the remaining components must be formed. Repeated high-temperature processing complicates and increases the cost of cell fabrication, whereas sintering all SOFC components in a single thermal cycle (co-sintering) saves both energy and time.

The implementation of co-sintering for a heterogeneous multilayer structure with a predetermined morphology was fundamental in developing a method for fabricating SOFCs using polymer-ceramic films followed by their co-sintering. This approach allowed for precise control over the thickness of the functional layers. Moreover, the use of nanoscale electrolyte powders—which significantly influence the kinetics of sintering without altering other physical properties such as the coefficient of thermal expansion, conductivity, and others—enabled the successful co-sintering of the SOFC components.

2. Synthesis of the initial powders

2.1. Synthesis of electrolyte nanopowders

Nanometer-sized powders of electrolyte materials $Zr_{0.84}Y_{0.16}O_{2-\delta}$ (YSZ), $Zr_{0.81}Sc_{0.19}O_{2-\delta}$ (ScSZ) and $Ce_{0.73}Gd_{0.27}O_{2-\delta}$ (GDC) were produced by laser evaporation [5]. The targets from which the nanopowders were generated were prepared using the following starting materials: YSZ powder obtained via solid-phase synthesis; a mechanical mixture of the simple oxides Sc_2O_3 and ZrO_2 in a mass ratio of 0.114; and a mechanical mixture of the simple oxides Gd_2O_3 and CeO_2 in a mass ratio of 0.381. The targets were fabricated using a uniaxial static press and sintered at 1300 °C for 1 h. They were formed as disks with a diameter of approximately 60 mm and a height of approximately 20 mm. The nanopowders were produced using an ytterbium fiber laser LK-1, equipped with a Riedel PC-41.02-KE-S chiller and an Optoskand d25 f60/200 optical head. A modulated (impulse-periodic) operating mode was employed, with a frequency of 5 kHz and a pulse duration of 100 μs. The radiation power was 450 W, and the wavelength was 1.07 μm. The nanopowders were obtained in an air atmosphere at a pressure of 1 atm.

The synthesized powders were annealed at 1000 °C for 4 h to achieve slight particle coarsening. The subsequent investigations into thermal properties, conductivity, and the fabrication of samples for determining electrode characteristics were carried out using these annealed powders.

2.2. Synthesis of cathode material powders

The cathode material powder $La_{0.7}Sr_{0.3}MnO_3$ (LSM) was obtained by pyrolyzing a polymer-salt composition (polyvinyl alcohol and nitrate salts) [6]. The starting reagents were $La(NO_3)_3$ (analytical grade), $Sr(NO_3)_2$ (reagent grade), and $Mn(NO_3)_2$ (analytical grade). A stoichiometric mixture of the reagents was dissolved in distilled water with the addition of polyvinyl alcohol (grade 11/2) in a polymer-to-salt ratio of 2. The resulting solution was heated in a porcelain crucible until the water was removed and the pyrolysis of polyvinyl alcohol commenced. In the final stage of the synthesis, the reaction mixture was calcined at 1100 °C for 10 h.

Three compositions of lanthanum strontium cobalt ferrite with varying chemical compositions were selected for the study: $La_{1-x}Sr_xCo_{1-y}Fe_yO_{3-\delta}$ (x = 0.2, 0.4; y = 0.2, 0.8). A commercial powder of $La_{0.6}Sr_{0.4}Co_{0.8}Fe_{0.2}O_{3-\delta}$ (LSCF-4080) was produced by Kceracell Co., Ltd., while powders of $La_{0.8}Sr_{0.2}Co_{0.2}Fe_{0.8}O_{3-\delta}$ (LSCF-2020) and $La_{0.6}Sr_{0.4}Co_{0.2}Fe_{0.8}O_{3-\delta}$ (LSCF-4020) were synthesized using the Solution Combustion Synthesis (SCS) method.

The starting reagents were La_2O_3 (analytical grade), $SrCO_3$ (analytical grade), $Fe(NO_3)_3$ (analytical grade), and $Co(NO_3)_2$ (reagent grade). The corresponding amounts of La_2O_3 and $SrCO_3$ were dissolved in a 0.1 N HNO_3 solution, while $Fe(NO_3)_3$ and $Co(NO_3)_2$ were dissolved in water until homogeneous solutions were obtained. Glycine (AMK Ltd, Russia) and/or citric acid of analytical grade (Weifang Ensigh Industry Co. Ltd, China) were used as combustible organic substances in amounts sufficient to sustain the combustion reaction in a reducing combustion regime.

The reaction products were milled and then sequentially calcined at 850 °C for 5 h, 950 °C for 5 h, and 1150 °C for 7 h to remove residual organic phases and to form the crystalline structure.

2.3. Synthesis of NiO nanopowder for the anode

The NiO nanopowder was obtained using the wire explosion method [7], which is a high-energy metal dispersion process resulting from a rapid phase transition. This method is based on an abrupt change in the physical state of the metal due to intense energy release when a high-density pulsed current (10^4–10^6 A·mm^{-2}) is passed through the wire. As a

result, the wire is instantaneously heated to temperatures exceeding the metal's boiling point, leading to the formation of a plasma state, subsequent evaporation, expansion, and condensation of particles into a nanopowder. The duration of the energy impact is approximately 10^{-5}–10^{-7} s, which prevents significant particle agglomeration and promotes the formation of a nanostructured material.

Nickel wire of grade NP2 (99.5% Ni) with a diameter of 100 μm was used as the raw material for NiO nanopowder synthesis. The energy source consisted of a discharge circuit with an inductance of 0.5 μH and a capacitor bank with a capacitance of 3.1 μF. The charging voltage was 10 kV. The wire explosion process was carried out at atmospheric pressure in a gas medium containing a mixture of nitrogen (N_2) and oxygen (O_2), ensuring oxidation of the generated nickel particles and the formation of nickel oxide (NiO) nanopowder [8].

The obtained powder exhibited predominantly spherical particle morphology with a narrow size distribution. The high degree of dispersion was achieved due to rapid cooling in the gas medium, while additional control over composition and phase was performed by varying the discharge parameters and gas mixture composition. This method enables the production of high-purity NiO nanopowder with controlled structural characteristics, making it a promising material for use as an anode component in solid oxide fuel cells.

3. Powder certification

The phase composition of the studied materials was determined by X-ray phase analysis [9] performed on a D8 DISCOVER diffractometer using copper radiation (Cu $K_{\alpha 1,2}$ $\lambda = 1.542$ Å) with a graphite monochromator on the diffracted beam. Data processing was carried out using TOPAS 3 software with the Rietveld refinement algorithm for structural parameters. A correction factor of $K = 0.89$ (in the Scherrer formula) was used for the estimation of the average crystallite size.

The specific surface area of the powders was determined by low-temperature nitrogen vapor adsorption using the BET method on an automatic TriStar 3000 analyzer. Assuming that the powder particles are spherical, the average particle size was calculated using the following formula:

$$d_{BET} = \frac{6}{\gamma_{theor} S_{BET}} \quad (1)$$

where d_{BET} - is the average particle diameter, S_{BET} is the specific surface area, and γ_{theor} is the theoretical density of the powder material. The morphology of the obtained powders was investigated using electron microscopy with a JEOL JEM 2100 transmission electron microscope and LEO 982, JEOL JSM-6390LA scanning electron microscopes.

3.1. Phase composition

X-ray spectroscopy data for the powders of the studied materials are presented in Figs. 1–3. All

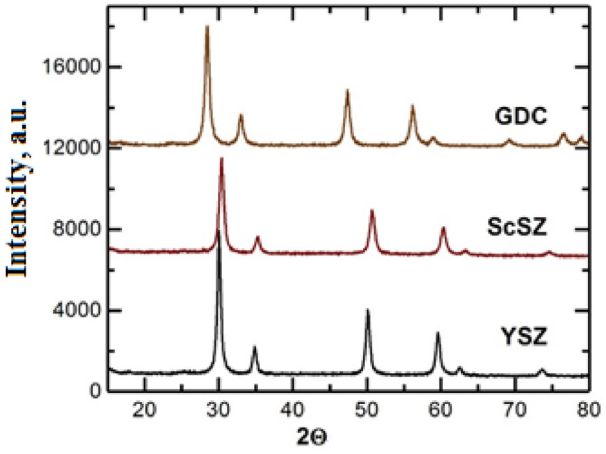

Fig. 1. Diffractograms of electrolyte material powders: YSZ, ScSZ, and GDC.

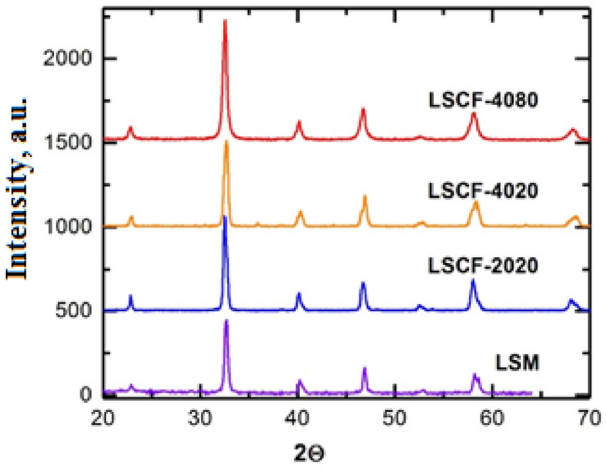

Fig. 2. Diffractograms of LSM and LSCF cathode material powders.

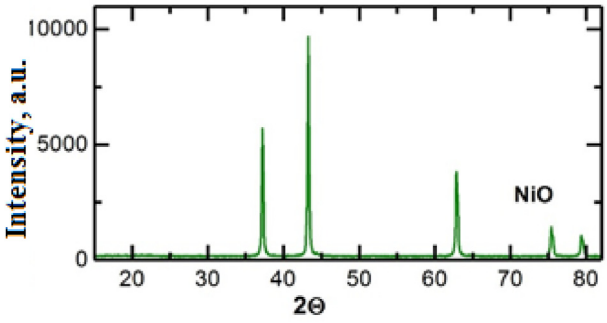

Fig. 3. Diffractogram of NiO powder.

electrolyte powders—YSZ, ScSZ, and GDC (Fig. 1) - are single-phase and represent solid solutions with the space group Fm-3m. X-ray phase analysis (Fig. 2) showed that the main phase of the LSM powder is rhombohedral (space group R-3c). Additionally, approximately 9 wt. % of a secondary LSM phase with orthorhombic symmetry (space group Pnma) was observed alongside the main phase. Lanthanum strontium cobalt ferrites are also characterized by a rhombohedral structure (space group R-3c). Meanwhile, the LSCF powders were single-phase with traces of secondary phases that disappeared after calcination above 1200 °C. The NiO nanopowder is single-phase (Fig. 3) and has a cubic lattice with the space group Fm-3m [10]. The powder characteristics are summarized in Table 1.

3.2. Powder morphology

Fig. 4 shows microphotographs of the original powders of solid electrolytes YSZ, ScSZ, and GDC. The

Table 1. Characteristics of the initial powders.

Powder	S_{BET}, m^2/g	d_{BET}, μm	Space group	Lattice parameter, Å	γ_{XRD}, g/sm^3
YSZ	65.3	15.5	Fm-3m	a = 5.143	5.94
ScSZ	97.4	11.0	Fm-3m	a = 5.087	5.70
GDC	34.2	0.02	Fm-3m	a = 5.424	7.25
LSM	2.13	0.43	R-3c	a = 5.510, c = 13.320	6.51
LSCF-2020	2.98	0.31	R-3c	a = 5.501. c = 13.407	6.60
LSCF-4020	0.46	2.05	R-3c	a = 5.481. c = 13.382	6.36
LSCF-4080	11.8	0.08	R-3c	a = 5.493. c = 13.453	6.50
NiO	15.6	0.05	Fm-3m	a = 4.178	7.45

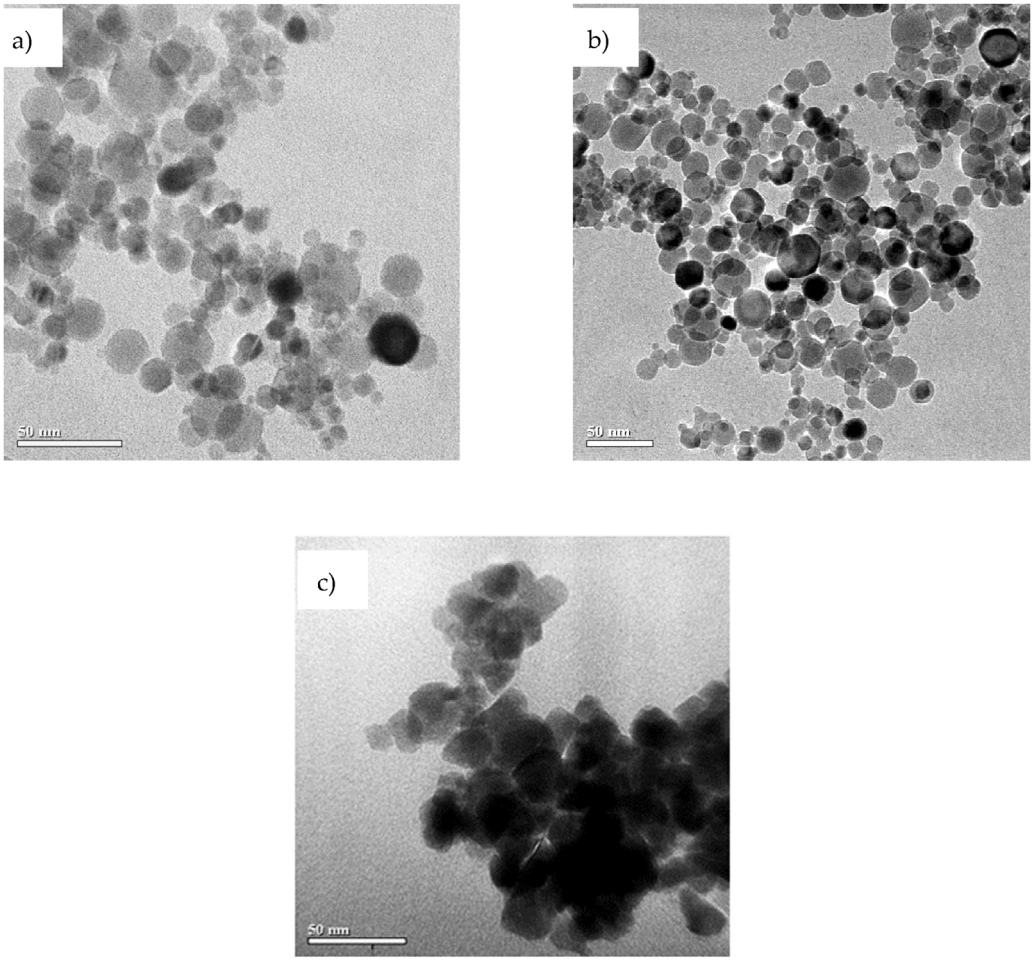

a) YSZ, b) ScSZ and c) GDC

Fig. 4. Microphotographs of the original solid electrolyte powders.

particles of the ZrO_2-based powders produced by the laser evaporation method are nearly spherical in shape, while the GDC powder particles are more like cubes with rounded edges. Moreover, microscopy confirms the estimated average particle sizes based on S_{BET}: approximately 15 nm for YSZ, 10 nm for ScSZ, and 25 nm for GDC [11].

Microphotographs of the cathode material powders are presented in Fig. 5. The LSM powder particles are coral-like with a spongy structure. In contrast, the particles of the powders produced by the SCS method appear as irregular agglomerates. The average particle sizes determined by the BET method correlate with the microscopy data (Table 1), with the exception of the LSM powder, for which the d_{BET} value is significantly smaller than the actual particle size. This discrepancy is due to the morphology of the LSM powder particles: their surface area, owing to the presence of pores and cavities, is considerably larger than that of monolithic particles [12–14].

The NiO nanopowder (Fig. 6), produced by the wire explosion method [15], also consists of spherical particles. The estimates of the average particle size obtained from microscopic data and specific surface area measurements are similar. However, the micrographs show that the particle size distribution is quite broad.

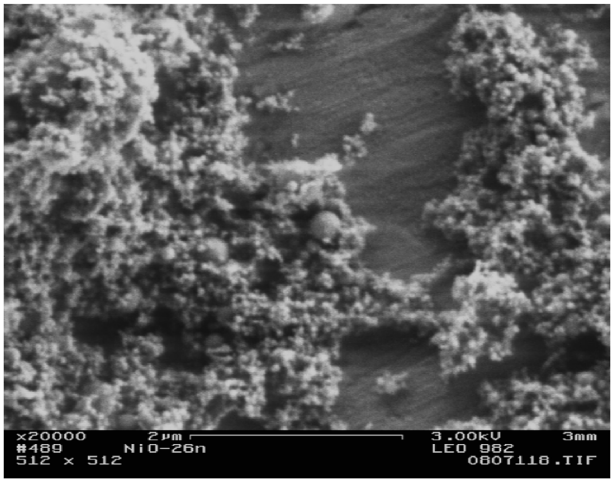

Fig. 6. Microphotograph of NiO nanopowder.

3.3. Chemical interaction of LSCF and GDC

It is known that the YSZ electrolyte is less chemically stable with respect to cathode materials than GDC [16]. That is why GDC is used as a buffer layer. However, literature data confirming the absence of interaction with GDC at high temperatures are not available for all LSCF compositions. Therefore, the chemical interaction between the selected LSCF compositions and GDC was investigated at 1200 and 1300 °C.

The initial LSCF and GDC powders were mixed in a 1:1 weight ratio. To achieve homogeneity, the powders were thoroughly blended using a disperser and a gravitational mixer for two days. The samples, pressed from the resulting composites, were sintered at 1200 and 1300 °C with a dwell time of 10 h at the peak temperature. The phase compositions of the sintered samples were analyzed using a D8 Discover diffractometer.

Fig. 7 presents the diffractograms of the initial powders and the composites sintered at different temperatures. X-ray phase analysis (XRD) of the composites did not reveal the formation of any secondary phases. However, it should be noted that the lattice parameters of the composite components change with increasing sintering temperature.

As an example, Table 2 presents data for the composite based on LSCF-4080.

The unit cell of GDC expands, while the unit cell volume of the electrode materials decreases, which is attributed to the diffusion of cations from the cathode material into the electrolyte. The increase in the lattice parameter of GDC is presumably due to the

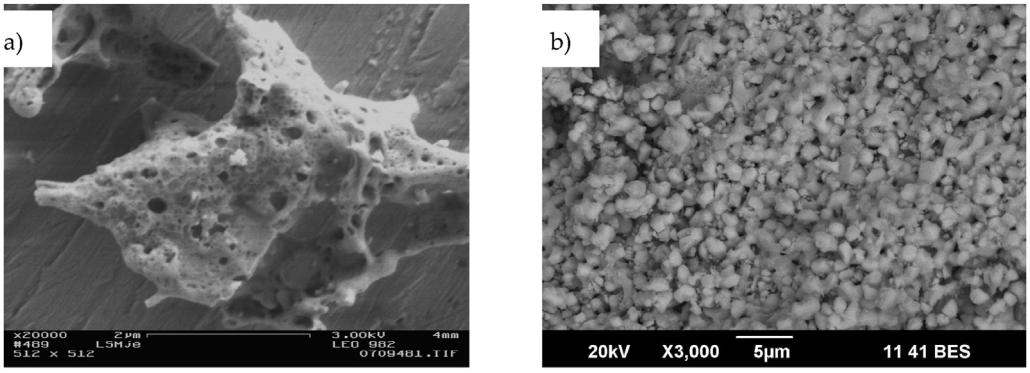

a) LSM, b) LSCF-4020

Fig. 5. Microphotographs of the original cathode material powders.

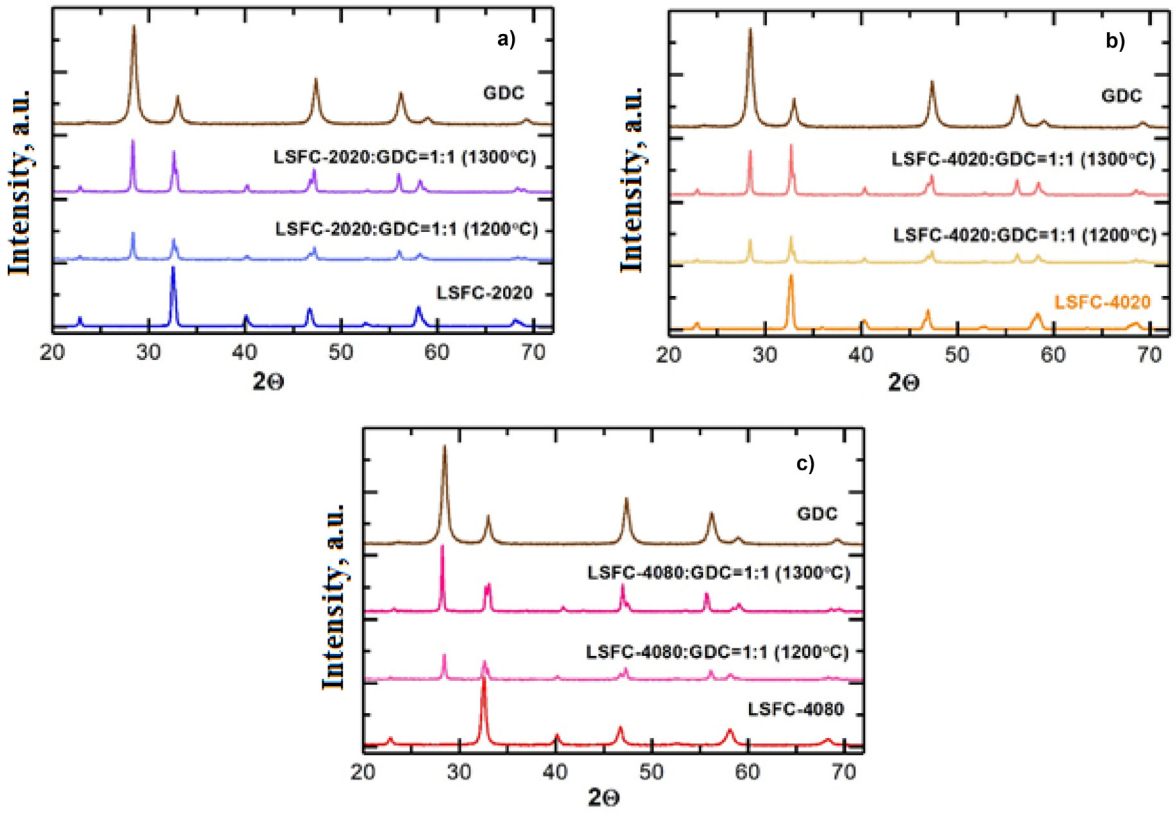

Cathode materials: a) LSCF-2020, b) LSCF-4020, c) LSCF-4080

Fig. 7. Diffractograms of the initial materials and composites calcined at 1200 and 1300 °C for 10 Hours.

Table 2. XRD data for the components of the LSCF-4080:GDC = 1:1 composite sintered at different temperatures.

Sintering temperature (°C)	Lattice parameter, Å	
	GDC	LSCF-4080
Initial	a = 5.424	a = 5.493, c = 13.453
1200	a = 5.432	a = 5.503, c = 13.400
1300	a = 5.435	a = 5.503, c = 13.405

incorporation of lanthanum and/or strontium cations into the fluorite lattice. In contrast, the incorporation of cobalt and/or iron should have led to a reduction in the GDC unit cell size due to their smaller ionic radii. However, the diffusion of transition metals into the electrolyte structure is possible along grain boundaries [17,18].

4. Conclusion

Nanoscale electrolyte powders $Zr_{0.84}Y_{0.16}O_2$-δ (YSZ), $Zr_{0.81}Sc_{0.19}O_2$-δ (ScSZ), and $Ce_{0.73}Gd_{0.27}O_2$-δ (GDC) were successfully synthesized using the laser evaporation method. Cathode materials were obtained through two different synthesis approaches: $La_{0.7}Sr_{0.3}MnO_3$ (LSM) powder was produced via pyrolysis of a polymer-salt composition, while lanthanum strontium cobalt ferrite powders $La_{0.8}Sr_{0.2}Co_{0.2}Fe_{0.8}O_3$-δ (LSCF-2020) and $La_{0.6}Sr_{0.4}Co_{0.2}Fe_{0.8}O_3$-δ (LSCF-4020) were synthesized using the Solution Combustion Synthesis method. Additionally, a commercial $La_{0.6}Sr_{0.4}Co_{0.8}Fe_{0.2}O_3$-δ powder was included in the study. The anode material, NiO nanopowder, was obtained using the wire explosion method.

Comprehensive characterization of the synthesized powders was conducted using X-ray phase analysis and electron microscopy. The results confirmed that all powders, except for LSM, which contained approximately 9 wt.% of a secondary phase, exhibited a single-phase composition. The electrolyte materials YSZ, ScSZ, GDC, and NiO were found to have a cubic lattice with the space group Fm-3m, while LSCF powders and the primary phase of LSM demonstrated a rhombohedral structure (space group R-3c). Morphological analysis revealed that YSZ, ScSZ, GDC, and NiO powders exhibited near-spherical particle shapes, whereas LSCF and LSM powders consisted of irregularly shaped particles. Furthermore, X-ray phase analysis confirmed the absence of chemical interaction between LSCF and GDC at 1300 °C, indicating their compatibility for potential co-sintering applications.

This study provides valuable insights into the structural and morphological properties of electrolyte, cathode, and anode materials, contributing to the development of optimized solid oxide fuel cell components.

Funding

This research was funded by the grant with reference number BR21882359, provided by the Ministry of Science and Higher Education of Kazakhstan.

Conflict of interest

The authors declare no conflicts of interest.

References

[1] V.V. Osipov, Yu.A. Kotov, M.G. Ivanov, E. Azarkevich, et al., Laser synthesis of oxide nanopowders, Laser Phys 16 (1) (2006) 116—125, https://doi.org/10.1134/S1054660X06010105.
[2] Fuel cell handbook, EG&G Technical Services, Inc., 2004, p. 427.
[3] B. Sudhasatwa, Recent Trends in Fuel Cell Science and Technology, Anamaya Publishers, New Delhi, 2007, p. 375.
[4] E.V. Tsipis, V.V. Kharton, Electrode materials and reaction mechanisms in solid oxide fuel cells: a brief review, J Solid State Electrochem 12 (2008) 1039—1060, https://doi.org/10.1007/s10008-007-0468-0.
[5] A.D. Maksimov, E.I. Azarkevich, I.V. Beketov, et al., Comparative analysis of craters formed on cathode and anode spots of a spark discharge in air on iron electrodes, Bull Russ Acad Sci Phys 87 (Suppl. 2) (2023) S274—S280, https://doi.org/10.1134/S1062873823704725.
[6] A.A. Ostroushko, Yu.V. Mogil'nikov, K.A. Popov, Thermal destruction of polymer-salt compositions containing d-metals in the form of oxygen-bearing anions, Inorg Mater 36 (6) (2000) 603—611, https://doi.org/10.1007/bf02757963.
[7] Y.A. Kotov, A.V. Bagazeyev, I.V. Beketov, et al., Properties of nickel oxide nanopowders prepared by electrical explosion of a wire, Tech Phys 50 (2005) 1279—1283, https://doi.org/10.1134/1.2103272.
[8] T.V. Terziyan, A.P. Safronov, A.V. Petrov, N.S. Volodina, I.V. Beketov, Effect of the chemical nature of metal oxide on adhesion to the polyacrylate matrix in filled nanocomposites, Russ J Phys Chem A 88 (8) (2014) 1300—1306, https://doi.org/10.1134/s0036024414060302.
[9] J.W. Fergus, Electrolytes for solid oxide fuel cells, J Power Sources 162 (1) (2006) 30—40, https://doi.org/10.1016/j.jpowsour.2006.06.062.
[10] O. Yamamoto, Electrical conductivity of stabilized zirconia with ytterbia and scandia, Solid State Ionics 79 (1995) 137—142, https://doi.org/10.1016/0167-2738(95)00044-7.
[11] S.P.S. Badwal, F.T. Ciacchi, D. Milosevic, Scandia—zirconia electrolytes for intermediate temperature solid oxide fuel cell operation, Solid State Ionics (1—2) (2000) 91—99, https://doi.org/10.1016/S0167-2738(00)00356-8, 136—137.
[12] A.A. Taskin, A.N. Lavrov, Y. Ando, Achieving fast oxygen diffusion in perovskites by cation ordering, Appl Phys Lett 86 (9) (2005) 091910, https://doi.org/10.1063/1.1864244.
[13] D. Parfitt, A. Chroneos, J.A. Kilner, R.W. Grimes, Molecular dynamics study of oxygen diffusion in $Pr_2NiO_4+\delta$, Phys Chem Chem Phys 12 (25) (2010) 6834—6836, https://doi.org/10.1039/c001809k.
[14] Z. Liang, Erratum to solutions of indefinite equations, Adv Pure Math 10 (9) (2020) 540—544, https://doi.org/10.4236/apm.2022.124023.
[15] L. Dos Santos-Gómez, J.M. Porras-Vázquez, E.R. Losilla, D. Marrero-López, et al., LSCF-CGO nanocomposite cathodes deposited in a single step by spray-pyrolysis, J Eur Ceram Soc 40 (2020) 3080—3088, https://doi.org/10.1016/j.jeurceramsoc.2017.10.010.
[16] T. Kenjo, M. Nishiya, $LaMnO_3$ air cathodes containing ZrO_2 electrolyte for high temperature solid oxide fuel cells, Solid State Ionics 57 (3—4) (1992) 295—302, https://doi.org/10.1016/0167-2738(92)90161-h.
[17] J.-D. Kim, G.-D. Kim, J.-W. Moon, Y.-I. Park, H.-W. Lee, K. Kobayashi, M. Nagai, C.-E. Kim, Corrigendum to Characterization of LSM—YSZ composite electrode by AC impedance spectroscopy, Solid State Ionics 144 (3—4) (2001) 387, https://doi.org/10.1016/S0167-2738(01)01009-8.
[18] E.P. Murray, T. Tsai, S.A. Barnett, Oxygen transfer processes in $(La,Sr)MnO_3/Y_2O_3$-stabilized ZrO_2 cathodes: an impedance spectroscopy study, Solid State Ionics 110 (3—4) (1998) 235—243, https://doi.org/10.1016/S0167-2738(98)00142-8.